

# A level-set numerical framework for the modeling of diffusive solid - solid phase transformation in the context of austenite decomposition

N. Chandrappa<sup>1</sup>, M. Bernacki<sup>1</sup>

<sup>1</sup> Mines-ParisTech, PSL-Research University, CEMEF – Centre de mise en forme des matériaux, CNRS UMR 7635, CS 10207 rue Claude Daunesse, Sophia Antipolis, France, {nitish.chandrappa,marc.bernacki}@mines-paristech.fr

**Résumé** — A full-field numerical framework using the level-set method has been developed to simulate diffusive solid-solid phase transformation at the mesoscopic scale in the context of austenite decomposition. A pseudo-1D test case with a planar interface is considered as a first case to demonstrate coherency in the results in terms of the expected steady states achieved. The ability of the numerical framework to model other diffusive solid state phenomena such as Ostwald ripening is successfully illustrated with a suitable test case.

**Keywords** — Full-field method, level-set, diffusive phase transformation.

## 1 Introduction

All strategic industries (aeronautics, nuclear, automotive, oil & gas, defense and renewable energies) make extensive use of metallurgical products. Under the pressure of intense international competition, there is an increasing demand from these industries to have more physically realistic models at their disposal to precisely predict the microstructural evolutions during thermomechanical treatments (TMTs) or thermal treatments (TTs), which in turn determine the in-service material performances. Thanks to the explosion of computer capacities, mesoscopic modeling techniques for metallic materials at the solid-state are now available. These lower scale approaches, the so-called full-field models, are based on a full description of the microstructure topology and have demonstrated an exciting potential for an extensive range of microstructure evolutions like the precise modeling of recrystallization (ReX) in dynamic (DRX) or post-dynamic (PDRX) conditions, grain growth (GG), diffusive solid-solid phase transformation (DSSPT), spheroidization and sintering. The main numerical frameworks involved are Monte Carlo Potts (MC) [1], Cellular Automata (CA) [2], Phase Field (PF) or MultiPhase Field (MPF) [3, 4], Front-Tracking [5, 6]/Vertex [7], and Level-Set (LS) models [8, 9]. These numerical methods are currently used and developed by many researchers [11] and regularly compared for particular metallurgical mechanisms. However, a global mesoscopic numerical approach allowing to model all these mechanisms in a unified framework remains to be developed. One of the objectives of this work is to implement such a unified framework.

In the context of full field numerical modeling of diffusive solid-solid phase transformation (SSPT), phase field (PF) [12, 13, 14, 15] methods are very popular and largely used. The diffuse interface description in PF methods naturally smoothens any material discontinuities across the interface. This is especially desirable in the resolution of a diffusion equation as there is no explicit consideration of interface jump conditions due to the discontinuities, and a single equation is resolved in the whole domain. However the presence of numerical parameters linked to the phase-field thickness can also bring difficulties in PF simulations, especially when the considered interfaces present largely anisotropic characteristics. On the other hand, LS have been extensively used for simulating ReX and GG mechanisms. LS approaches, unlike PF methods, do not introduce any artificial thickness of the interface and is based on a kinetic description of the interface network migration, i.e. do not deal directly with the minimization of the energy of the considered system. This kinetic description provides an easy and a natural way to model concomitant mechanisms and take into account the influence of both grain and phase interfaces seamlessly.

So, the central idea of this work is to develop a LS numerical framework to model diffusive SSPT, illustrated here in the context of austenite decomposition (austenite to ferrite transformation) in steels. In addition, a transition to diffuse interface description is adopted for the resolution of diffusion equation to avoid explicit consideration of interface jump conditions. In other words, for interface description and migration, a LS-based convective/diffusive framework is developed, while for the resolution of solute diffusion equation, a PF like diffuse interface description is adopted.

## 1.1 Numerical formalism

Thanks to the phase field like diffusive description of the interface, the total solute diffusion flux ( $\mathbf{J}$ ) can be expressed as a continuous field through a sum of fluxes of each phase (denoted  $\gamma$  for austenite and  $\alpha$  for ferrite) weighted by the PF order parameter ( $\phi$ ) :

$$\mathbf{J} = \phi \mathbf{J}_\alpha + (1 - \phi) \mathbf{J}_\gamma, \quad (1)$$

Likewise, the total carbon concentration field ( $C$ ) can also be expressed as a continuous variable :

$$C = \phi C_\alpha + (1 - \phi) C_\gamma, \quad (2)$$

A constant concentration ratio is imposed at the diffuse interface composing the mixture of two phases. This condition ensures that the redistribution of the solute atoms between the two phases at the interface respects a partitioning ratio ( $k$ ) equal to that at the equilibrium :

$$k = \frac{C_\alpha}{C_\gamma} = \frac{C_\alpha^{eq}}{C_\gamma^{eq}}, \quad (3)$$

where  $C_\alpha^{eq}$  and  $C_\gamma^{eq}$  are the carbon equilibrium concentrations of  $\alpha$  and  $\gamma$  phases at temperature  $T$ .

Following Fick's laws of diffusion, the diffusion equation for carbon partitioning can be expressed as :

$$\begin{aligned} \frac{\partial C}{\partial t} &= -\nabla \cdot \mathbf{J} = -\nabla \cdot [\phi(-D_\alpha^C \nabla C_\alpha) + (1 - \phi)(-D_\gamma^C \nabla C_\gamma)], \\ \frac{\partial C}{\partial t} &= \nabla \cdot [\phi D_\alpha^C \nabla C_\alpha + (1 - \phi) D_\gamma^C \nabla C_\gamma], \end{aligned} \quad (4)$$

Invoking Eq. (2) and (3), a modified carbon diffusion equation [14, 16] is obtained :

$$\frac{\partial C}{\partial t} = \nabla \cdot \left\{ D^*(\phi) \left[ \nabla C - \frac{C(k-1)}{1+\phi(k-1)} \nabla \phi \right] \right\}, \quad (5)$$

where  $D^*(\phi)$  is called "mixed diffusivity" and is defined as,

$$D^*(\phi) = \frac{D_\gamma^C + \phi(kD_\alpha^C - D_\gamma^C)}{1 + \phi(k-1)}.$$

With further simplifications, the above diffusion equation (5) can be transformed into a Convective-Diffusive-Reactive (CDR) form as follows :

$$\begin{aligned} \frac{\partial C}{\partial t} &= \nabla \cdot [D^*(\phi) \nabla C - CA(\phi)] \\ \frac{\partial C}{\partial t} + (\mathbf{A} - \nabla D^*) \cdot \nabla C - D^* \Delta C + RC &= 0, \end{aligned} \quad (6)$$

where,

$$\mathbf{A}(\phi) = \frac{D^*(\phi)(k-1)}{1 + \phi(k-1)} \nabla \phi.$$

Let  $\varphi \in H_0^1(\Omega)$  be a test function, we obtain for the weak formulation of Eq. (6) :

$$\int_{\Omega} \frac{\partial C}{\partial t} \phi d\Omega + \int_{\Omega} (\mathbf{A} - \nabla D^*) \cdot \nabla C \phi d\Omega - \int_{\Omega} D^* \Delta C \phi d\Omega + \int_{\Omega} RC \phi d\Omega = 0. \quad (7)$$

Applying divergence theorem and imposing Neumann boundary conditions on the boundaries of the computational domain,  $\nabla C \cdot \mathbf{n}|_{\partial\Omega} = 0$  :

$$\int_{\Omega} D^* \Delta C \phi d\Omega = \int_{\partial\Omega} \phi D^* \nabla C \cdot \mathbf{n} dS - \int_{\Omega} \nabla(D^* \phi) \cdot \nabla C d\Omega = - \int_{\Omega} \nabla(D^* \phi) \cdot \nabla C d\Omega.$$

Substituting the above term in Eq. (7), we get after simplification :

$$\int_{\Omega} \frac{\partial C}{\partial t} \phi d\Omega + \int_{\Omega} \mathbf{A} \cdot \nabla C \phi d\Omega + \int_{\Omega} D^* \nabla \phi \cdot \nabla C d\Omega + \int_{\Omega} RC \phi d\Omega = 0. \quad (8)$$

The above CDR equation was implemented in a *P1* finite element (FE) framework [10]. It can be highlighted that compared to the strong formulation in Eq. (6), the gradient of the mixed diffusivity term ( $\nabla D^*$ ) vanishes in the weak formulation. In terms of numerical stability, this is of great interest considering the abrupt evolution of this term in the phase interface.

It has been shown that the phase field order parameter has a steady state solution [14] of the following form :

$$\phi = \frac{1}{2} \tanh\left(-\frac{3\psi}{\eta}\right) + \frac{1}{2}, \quad (9)$$

where  $\psi$  represents a signed Euclidean distance to the interface that we will consider as the LS of interest in the following as illustrated in fig 1a. This hyper tangent relation is central to the transition between a diffusive and a level-set description of the interface. So, following the resolution of the diffusion equation, we go back to the LS description of the interface and the interface migration is then governed by the resolution of a kinetic equation applied to the LS function with a prescribed velocity field ( $\mathbf{v}$ ) :

$$\begin{cases} \frac{\partial \psi}{\partial t} + \mathbf{v} \cdot \nabla \psi = 0 \\ \psi(\mathbf{x}, t = 0) = \psi_0(\mathbf{x}) \end{cases} \quad (10)$$

At the mesoscopic scale, for solid state phenomena such as recrystallization (ReX) and SSPT, interface kinetics,  $\mathbf{v}$ , is classically defined through the following relation [17, 11] :

$$\mathbf{v} = \mu F \mathbf{n}, \quad (11)$$

where  $\mu$  is the mobility of the considered interface,  $F$  the global driving force accounting for the considered phenomena, and  $\mathbf{n}$  is the outward unit normal vector to the considered interface.

Typically, the principal component of the driving force is the difference in the Gibbs free energy between the different phases ( $\Delta G$ ). In addition, the presence of grain and phase interfaces introduce capillarity effects through the minimization of surface energy (well known as the Gibbs-Thomson effect). The contribution of strain energy due to deformation ( $\llbracket E \rrbracket$ ) can also be incorporated in the same kinetic framework. It should be highlighted that the  $\Delta G$  component does not vanish only across phase interfaces (boundary between two different phases). So, in order to accommodate various contributions coming from different types of interfaces in the same framework, characteristic functions specific to the interface ( $\chi_{\gamma\alpha}$ ,  $\chi_{\gamma\gamma}$ , and  $\chi_{\alpha\alpha}$ ) can be adopted. Thus, the generalized net driving force and the net kinetics could be formulated as :

$$F = \chi_{\gamma\alpha} (\Delta G - \kappa \sigma_{\gamma\alpha} + \llbracket E \rrbracket_{\gamma\alpha}) + \chi_{\gamma\gamma} (-\kappa \sigma_{\gamma\gamma} + \llbracket E \rrbracket_{\gamma\gamma}) + \chi_{\alpha\alpha} (-\kappa \sigma_{\alpha\alpha} + \llbracket E \rrbracket_{\alpha\alpha}), \quad (12)$$

$$\begin{aligned} \mathbf{v} = & \chi_{\gamma\alpha} \mu_{\gamma\alpha} (\Delta G - \kappa \sigma_{\gamma\alpha} + \llbracket E \rrbracket_{\gamma\alpha}) \mathbf{n} + \chi_{\gamma\gamma} \mu_{\gamma\gamma} (-\kappa \sigma_{\gamma\gamma} + \llbracket E \rrbracket_{\gamma\gamma}) \mathbf{n} \\ & + \chi_{\alpha\alpha} \mu_{\alpha\alpha} (-\kappa \sigma_{\alpha\alpha} + \llbracket E \rrbracket_{\alpha\alpha}) \mathbf{n}, \end{aligned} \quad (13)$$

where  $\kappa$  is the trace of curvature tensor of the interface and  $\sigma$  is the interfacial energy, accounting for the Gibbs-Thomson effect.

Neglecting, at yet, the strain energy contribution for simplicity and prescribing the above velocity field into Eq. 10 yields :

$$\frac{\partial \psi}{\partial t} + \chi_{\gamma\alpha} \mu_{\gamma\alpha} \Delta G \mathbf{n} \cdot \nabla \psi - [\chi_{\gamma\alpha} \mu_{\gamma\alpha} \sigma_{\gamma\gamma} + \chi_{\gamma\gamma} \mu_{\gamma\gamma} \sigma_{\gamma\gamma} + \chi_{\alpha\alpha} \mu_{\alpha\alpha} \sigma_{\alpha\alpha}] \kappa \mathbf{n} \cdot \nabla \psi = 0 \quad (14)$$

By verifying the metric property of a distance function,  $\|\nabla \psi\| = 1$  all along the simulation, we can write :

$$\mathbf{n} = -\frac{\nabla \psi}{\|\nabla \psi\|} = -\nabla \psi \implies \kappa = \nabla \cdot \mathbf{n} = -\Delta \psi.$$

We can then rewrite Eq.14 in a convective-diffusive form to be resolved for interface migration :

$$\frac{\partial \psi}{\partial t} + \chi_{\gamma\alpha} \mu_{\gamma\alpha} \Delta G \mathbf{n} \cdot \nabla \psi - [\chi_{\gamma\alpha} \mu_{\gamma\alpha} \sigma_{\gamma\alpha} + \chi_{\gamma\gamma} \mu_{\gamma\gamma} \sigma_{\gamma\gamma} + \chi_{\alpha\alpha} \mu_{\alpha\alpha} \sigma_{\alpha\alpha}] \Delta \psi = 0. \quad (15)$$

After the resolution of the above equation, a suitable re-initialization procedure [18] is adopted to restore the metric property of the LS function at each time step.

## Description of $\Delta G$

In the above formalism,  $\Delta G$  is described based on a local linearization of the phase diagram as seen in the works of Mecozzi et al [14].  $\Delta G$  is basically assumed to be proportional to a small undercooling ( $\Delta T = T^{eq} - T$ ). With low undercooling assumptions, the variations of enthalpy ( $\Delta H$ ), and the entropy ( $\Delta S$ ) with temperature could be negligible ( $\Delta S^{eq} \approx \Delta S$ ,  $\Delta H^{eq} \approx \Delta H$ ). So the Gibbs free energy for phase change is defined as :

$$\Delta G(T, C) = \Delta S \Delta T.$$

Linearizing at a reference temperature ( $T^R$ ), and assuming only carbon element partitions, the  $\Delta G$  component is expressed as follows :

$$\Delta G(T, C) = \Delta S [(T^R - T) + 0.5m_{\gamma}^R (C_{\gamma} - C_{\gamma}^R) + 0.5m_{\alpha}^R (C_{\alpha} - C_{\alpha}^R)], \quad (16)$$

where  $C_{\alpha}^R$  and  $C_{\gamma}^R$  are the equilibrium carbon concentrations at  $T^R$  of ferrite and austenite respectively.  $m_{\alpha}^R$  and  $m_{\gamma}^R$  are the slopes of the boundary lines of the  $\alpha$  and  $\gamma$  phase respectively, linearized at  $T^R$ . These are deduced by thermodynamic evaluations using Thermo-Calc software [19]. With the help of eqs. (2) and (3), the above description could be further expressed as a function of  $C$  for each configuration of  $\phi(\mathbf{x}, t)$  :

$$\Delta G = \Delta S \left[ T^R - T + 0.5m_{\gamma}^R \left( \frac{C}{1 + \phi(k-1)} - C_{\gamma}^R \right) + 0.5m_{\alpha}^R \left( \frac{kC}{1 + \phi(k-1)} - C_{\alpha}^R \right) \right]. \quad (17)$$

Based on the same linearization, the equilibrium carbon concentrations of each phase can be estimated as follows :

$$C_i^{eq} = C_i^R + \frac{T - T^R}{m_i^R}, \quad \text{with } i = \{\alpha, \gamma\} \quad (18)$$

Using the above equations (18), the equilibrium partitioning ratio ( $k$ ) can be expressed at each temperature  $T$  as :

$$k = \frac{C_{\alpha}^R + \frac{T - T^R}{m_{\alpha}^R}}{C_{\gamma}^R + \frac{T - T^R}{m_{\gamma}^R}}. \quad (19)$$

## 2 Results and Analyses

As a first case, a pseudo-1D domain (slender 2D, fig. 1b) with a planar interface between one austenite grain and one ferrite grain is considered for austenite decomposition. The following assumptions are imposed :

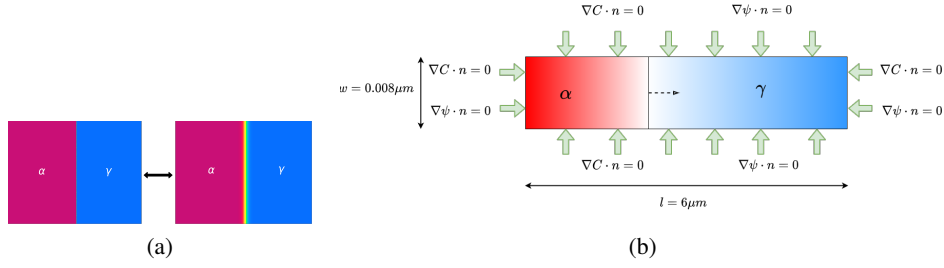


FIGURE 1 – (a) The level set of interest ( $\psi$  on the left side) and the corresponding diffuse phase field description ( $\phi$  on the right side), and (b) the pseudo-1D test case with one grain of each phase : red - ferrite, blue - austenite

- The transformation kinetics are assumed to be of **mixed mode character** with both interface and diffusion controlled modes. So, the concentration at the interface doesn't attain the equilibrium concentration right away, and the diffusion in the bulk of the phase is not instantaneous.
- **Para-equilibrium** conditions are imposed. Thus the partitioning of substitutional solute elements are neglected. Only carbon redistributes and contributes to the global driving pressure.
- The interface mobility is assumed to be homogeneous and isotropic.
- Cooling is assumed to be instantaneous, and the phase transformation takes place at isothermal conditions.

A set of fictitious data carefully chosen has been adopted for this case :

- **Initial conditions** : The initial condition is assumed to be at  $T^{initial} = 1120\text{ K}$  with the equilibrium concentrations,  $C_{\alpha}^{initial} = 0.005\text{ wt\%}$  and  $C_{\gamma}^{initial} = 0.113\text{ wt\%}$ . The interface position is imposed to be at  $2.5\ \mu\text{m}$  from the left boundary and is expected to migrate to the right during austenite decomposition.  $\eta$  is fixed to  $0.3\ \mu\text{m}$ .
- **Reference data** : The reference temperature for linearization of the phase diagram is assumed to be  $T^R = 1100\text{ K}$  with the equilibrium concentrations,  $C_{\alpha}^R = 0.01\text{ wt\%}$  and  $C_{\gamma}^R = 0.15\text{ wt\%}$ . Linearized slopes,  $m_{\alpha}^R = -10000\text{ K/wt\%}$  and  $m_{\gamma}^R = -200\text{ K/wt\%}$ , and entropy change,  $\Delta S = 4 \times 10^{-13}\text{ J/(K}\mu\text{m}^3)$ .
- **Simulating conditions** : For simplicity, the simulation temperature is assumed to be the same as the reference one,  $T = 1100\text{ K}$ . For the initial conditions assumed, this is equivalent to an instantaneous cooling of  $20\text{ K}$ . The simulation temperature is held isothermal throughout the phase transformation. Since the simulation temperature is equal to the reference one, the expected equilibrium concentrations at the steady state should be,  $C_{\alpha}^{eq} = 0.01\text{ wt\%}$  and  $C_{\gamma}^{eq} = 0.15\text{ wt\%}$ .
- Arrhenius type law is used for temperature dependence of mobility and the diffusivities with  $D_{\alpha}^0 = 2.2 \times 10^8\ \mu\text{m}^2/\text{s}$ ;  $D_{\gamma}^0 = 1.5 \times 10^7\ \mu\text{m}^2/\text{s}$ ;  $\mu_0 = 2 \times 10^{17}\ \mu\text{m}^4/(\text{Js})$ ;  $Q_{\alpha} = 122.5\text{ kJ/mol}$ ;  $Q_{\gamma} = 142.1\text{ kJ/mol}$ ; and  $Q_{\mu} = 140\text{ kJ/mol}$ .

A static isotropic mesh of  $2\text{ nm}$  is considered with a time step of  $1\text{ ms}$ .

From the expected equilibrium concentrations, it is possible to analytically estimate the expected steady position of the interface by applying mass conservation. For this pseudo-1D case, it is expected to be at  $3.514\ \mu\text{m}$ .

Fig. (2) shows the carbon profile evolution at selected time steps. It could be observed that, initially peaks are developed close to the interface in the austenite side indicating the solute enrichment during the transformation as the carbon atoms from the ferrite side diffuse into the austenite side. As steady state is reached, plain profiles start to develop indicating equilibrium. At steady state, the simulated equilibrium concentrations are found to be :  $C_{\alpha}^{eq, num} = 0.0099\text{ wt\%}$  and  $C_{\gamma}^{eq, num} = 0.1483\text{ wt\%}$ , which are close to the expected concentrations. On the other hand, Fig. (3) shows the interface kinetics where the interface position can be observed to converge to a steady value of  $\Gamma^{eq, num} = 3.47\ \mu\text{m}$  which is well within the range of the expected position, while the interface velocity tends towards 0 indicating convergence.

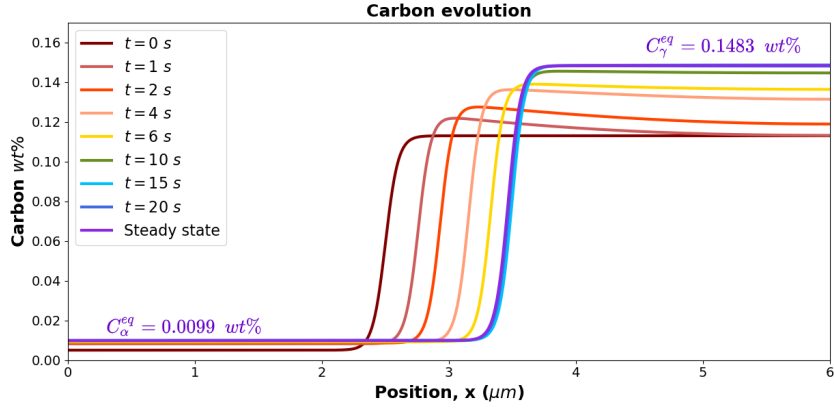


FIGURE 2 – Evolution of the carbon profiles from the initial to the steady state

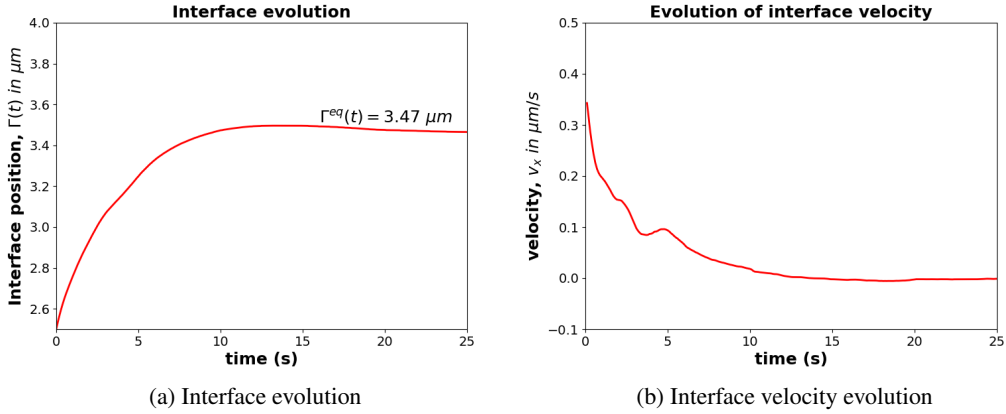


FIGURE 3 – Evolution of interface kinetics

## 2.1 Other diffusive solid state phenomena : Ostwald Ripening

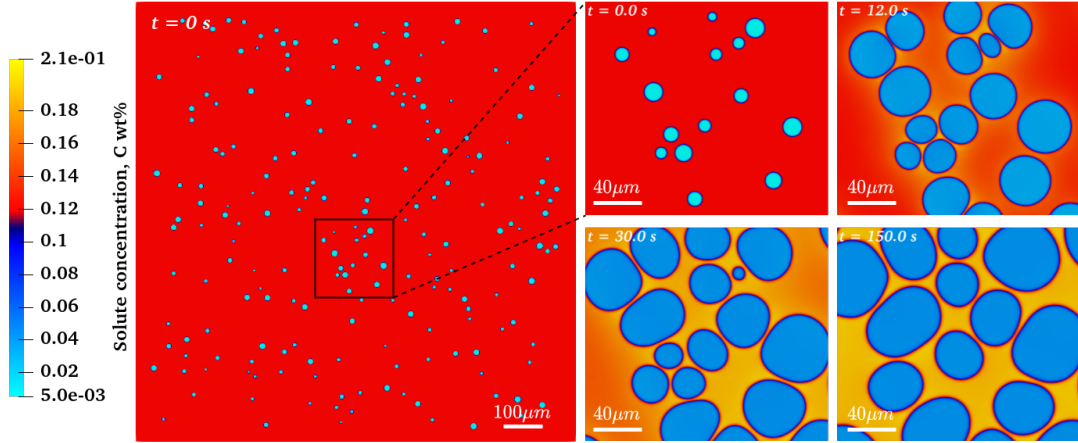
Using the same numerical framework, it is possible to simulate other diffusive solid state phenomena that are governed by similar components of driving pressure and kinetics. One such phenomenon is Ostwald ripening [20], in which larger second phase particles (SPPs) grow at the expense of smaller particles in a parent matrix (fig. 4a) towards the latter stage of a phase separation. Due to the Gibbs Thomson effects, the local equilibrium at the interface around a particle is affected. A concentration gradient is created between the multimodal SPPs due to the solute mass transport resulting from the capillarity effects. Owing to this, the smaller particles dissolve at the expense of coarsening of the larger ones. Thus, there is an increase in the mean particle size while a decrease in the total number of particles.

In order to simulate this phenomenon, a large square domain of size  $1000 \mu\text{m}^2$  with 200 particles of  $\alpha$  phase randomly distributed in the parent  $\gamma$  phase has been considered. The radii of the particles have been normally distributed within a range of  $2.5 - 7.5 \mu\text{m}$  with a mean size of  $5 \mu\text{m}$ . The following initial conditions were assumed :  $C_\alpha^i = 0.0005 \text{ wt}\%$ ;  $C_\gamma^i = 0.12 \text{ wt}\%$ ;  $T = T^R = 1100 \text{ K}$ ;  $C_\alpha^R = 0.045 \text{ wt}\%$  and  $C_\gamma^R = 0.2 \text{ wt}\%$ . Anisotropic adaptive remeshing has been employed for this case. In addition, the diffuse interface thickness ( $\eta$ ) and the remeshing parameters are also adapted to the mean particle size as they evolve through an appropriate affine relationship with the mean particle radius. A fixed time step of  $1 \text{ ms}$  has been considered. The particles have been represented by multi-level set functions using the coloration/ re-coloration scheme proposed in [21] to avoid numerical coalescence while limiting the number of level-set functions (a more costly strategy will consist of considering one LS function for each  $\alpha$  particle). In this context, in order to compute the phase field function for the diffuse interface description, the hyper-tangent relationship now becomes :

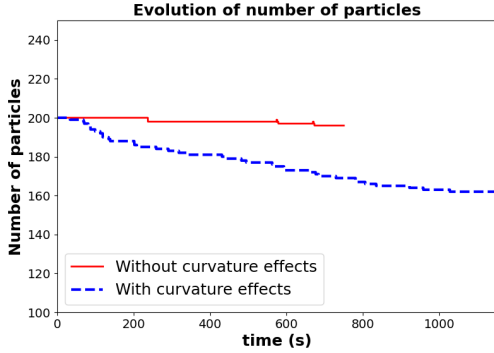
$$\phi = \frac{1}{2} \tanh \left( -3 \frac{\max_{i \in \{1, \dots, N_{LS}\}} \Psi_i}{\eta} \right) + \frac{1}{2}, \quad (20)$$

where  $N_{LS}$  is the total number of LS functions.

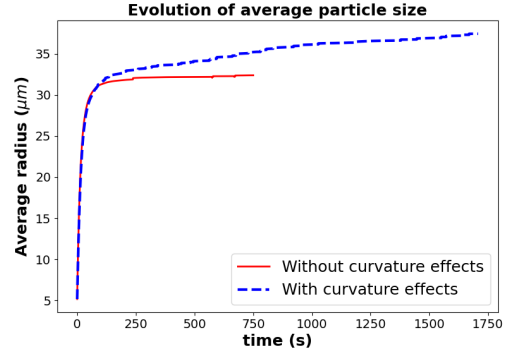
Fig. 4a shows the initial distribution of the matrix-precipitate system and the time evolution of the particles in a particular region. It can be observed that all the particles grow initially since  $\Delta G \gg \sigma\kappa$  during the initial stages. However as they tend towards local equilibrium for solute concentrations, curvature effects play significant role as larger particles continue to grow while there is dissolution of smaller particles, showing Ostwald ripening behavior. Fig. 4 further reiterates the monotonous decrease in the number of particles and the monotonous increase in the mean particle size observed for the case with Gibbs Thomson effects due to coarsening. While for the case without curvature effects, the mean particle size converges to a fairly constant value and is lower compared to the other case.



(a) Time evolution of SPPs- Zoomed on a few particles



(b) Time evolution of number of particles



(c) Time evolution of mean particle size

FIGURE 4 – Evolution of SPPs statistics with and without curvature effects

### 3 Conclusion and perspectives

A mixed diffuse interface - LS formalism was implemented in a finite element numerical framework to simulate diffusive solid-solid phase transformation. A pseudo-1D test case was considered with a fictitious data set to simulate isothermal phase transformation. The numerical model yielded coherent and expected results in terms of the steady states achieved. It was also demonstrated that other diffusive solid state phenomena such as Ostwald ripening can be easily simulated using the same numerical framework. It was shown that due to coarsening of the larger particles in the matrix, the mean particle size increases

in comparison to a case without curvature effects. As the particles evolve, adapting the diffuse interface thickness and the re-meshing parameters seem to improve computational performance while ensuring a smooth evolution of the interfaces. Thus, the numerical model seems to be promising and capable of simulating diffusive solid state phenomena. As a part of future work, the main idea is to consider multiphase polycrystals. The introduction of multiple junctions would then demand the need for special attention for the description of driving forces and the LS resolution at the multiple junctions. Introduction of cooling rate effects through continuous cooling curves will also be considered. Nucleation theories would also be introduced into the framework.

## Références

- [1] A. Rollett, D. J. Srolovitz, R. Doherty, and M. Anderson. *Computer simulation of recrystallization in non-uniformly deformed metals*, Acta Metallurgica, vol. 37, no. 2, pp. 627–639, 1989.
- [2] D. Raabe. *Cellular automata in materials science with particular reference to recrystallization simulation*, Annual Review of Materials Research, vol. 32, no. 1, pp. 53–76, 2002.
- [3] I. Steinbach, F. Pezzolla, B. Nestler, M. Seesselberg, R. Prieler, and J. Rezende. *A phase field concept for multiphase systems*, Physica D : Nonlinear Phenomena, vol. 94, pp. 135–147, 1996.
- [4] N. Moelans, B. Blanpain, and P. Wollants. *Quantitative analysis of grain boundary properties in a generalized phase field model for grain growth in anisotropic systems*, Physical Review B, vol. 78, no. 2, p. 024113, 2008.
- [5] S. Florez, K. Alvarado, D. P. Muñoz, and M. Bernacki, *A novel highly efficient lagrangian model for massively multidomain simulation applied to microstructural evolutions*, Computer Methods in Applied Mechanics and Engineering, vol. 367, p. 113107, 2020.
- [6] S. Florez, K. Alvarado, B. Murgas, N. Bozzolo, D. Chatain, C.E. Krill III, M. Wang, G.S. Rhorer, and M. Bernacki. *Statistical behaviour of interfaces subjected to curvature flow and torque effects applied to microstructural evolutions*, Acta Materialia, In press, 2021.
- [7] L. Barrales Mora, G. Gottstein, and L. Shvindlerman, *Three-dimensional grain growth : Analytical approaches and computer simulations*, Acta Materialia, vol. 56, no. 20, pp. 5915–5926, 2008.
- [8] B. Merriman, J. Bence, and S. Osher. *Motion of multiple junctions : A level set approach*, Journal of Computational Physics, vol. 112, pp. 334–363, 1994.
- [9] M. Bernacki, Y. Chastel, T. Coupez, and R. Logé, *Level set framework for the numerical modelling of primary recrystallization in polycrystalline materials*, Scripta Materialia, vol. 58, no. 12, pp. 1129–1132, 2008.
- [10] M. Bernacki, R.E. Logé, T. Coupez. *Level set framework for the finite-element modelling of recrystallization and grain growth in polycrystalline materials*, Scripta Materialia, 2011.
- [11] A. Rollett, G. S. Rohrer and J. Humphreys. *Recrystallization and Related Annealing Phenomena (Third Edition)*, Elsevier Science, 2017.
- [12] G. Pariser, P. Schaffnit, I. Steinbach, W. Bleck. *Simulation of the  $\gamma$ - $\alpha$ -transformation using the phase-field method*, Steel research, vol. 72, no. 9, pp. 354–360, 2001.
- [13] C-J. Huang, D. J. Browne, S. McFadden. *A phase-field simulation of austenite to ferrite transformation kinetics in low carbon steels*, Acta materialia, vol. 54, no. 1, pp. 11–21, 2006.
- [14] M. G. Mecozzi. *Phase field modelling of the austenite to ferrite transformation in steels*, PhD thesis, Delf University of Technology.
- [15] M. Militzer, M. Mecozzi, J. Sietsma, S. Van der Zwaag. *Three-dimensional phase field modelling of the austenite-to-ferrite transformation*, Acta materialia, vol. 54, no. 15, pp. 3961–3972, 2006.
- [16] J. Tiaden, B. Nestler, H-J. Diepers, I. Steinbach. *The multiphase-field model with an integrated concept for modelling solute diffusion*, Physica D : Nonlinear Phenomena, vol. 115, no. 1-2, pp. 73–86, 1998.
- [17] J. W. Christian. *The theory of transformations in metals and alloys*, Equilibrium and general kinetic theory, vol. 586, 1975.
- [18] M. Shakoor, B. Scholtes, P-O. Bouchard, M. Bernacki. *An efficient and parallel level set reinitialization method—application to micromechanics and microstructural evolutions*, Applied Mathematical Modelling, vol. 39, no. 23-24, pp. 7291–7302, 2015.
- [19] *Thermo-Calc Software*, <http://www.thermocalc.se/>.
- [20] P.W. Voorhees. *The theory of Ostwald ripening*, Journal of Statistical Physics, 38 :231–252, 1985.
- [21] B. Scholtes, M. Shakoor, A. Settefrati, P-O. Bouchard, N. Bozzolo, M. Bernacki. *New finite element developments for the full field modeling of microstructural evolutions using the level set method*, Computational Materials Science, vol. 109, 388–398, 2015.